In vivo magnetic resonance imaging and spectroscopy of Alzheimer__s disease in transgenic mice

Braakman, N.

2 Theoretical background: MRI and MRS

Without a basic knowledge of MRI physics, basic imaging phenomena, including the source of image contrast, relaxometry and 2D spectroscopy, would be very difficult to explain. This chapter gives a brief introduction of MR physics with emphasis on fast spin echo imaging, transverse relaxation mapping and 2D correlated spectroscopy.

MR is based upon the interaction between an applied magnetic field and a nucleus with a nuclear magnetic moment or "spin" (1-3). Several nuclei, including ^{1}H, ^{31}P, ^{13}C, ^{15}N, and ^{19}F have nuclear magnetic moments corresponding with spin ½ and are most suitable for detection by magnetic resonance (2-4). Protons are the most abundant spin ½ nuclei in living organisms and they have the best NMR sensitivity (2-4). For this reason protons are the most frequently studied nuclei. As a crude simplification, nuclear spins can be thought of as small magnets. When placed in an external magnetic field (B_0) a large number of proton spins will be aligned parallel to B_0, with a somewhat smaller number oriented anti-parallel. This orientation yields a net nuclear magnetization and a net magnetization vector M_z parallel to B_0 (Fig. 2.1a).

When tilted away from the magnetic field, the spins precess about the axis of B_0 (commonly taken as the z-axis) at a frequency proportional to the magnitude of the external field, according to

$$\nu_0 = {}^{\omega_0}\!/_{2\pi} = {}^{\gamma B_0}\!/_{2\pi}, \tag{2.1}$$

with ν_0 the Larmor frequency in MHz, and γ the gyromagnetic ratio. For protons $\gamma/2\pi$ = 42.576 MHz·Tesla^{-1}. When a second, time-dependent magnetic field (B_1) is applied perpendicular to B_0, by using an RF pulse at the Larmor frequency, the magnetization vector M_z will rotate away from the z-axis towards the xy-plane. The angle of rotation (α), or flip angle, of M_z around B_1 is defined as

$$\alpha = {}^{\gamma B_1 \tau}\!/_{2\pi}, \tag{2.2}$$

with τ the time during which the RF pulse field B_1 is switched on.

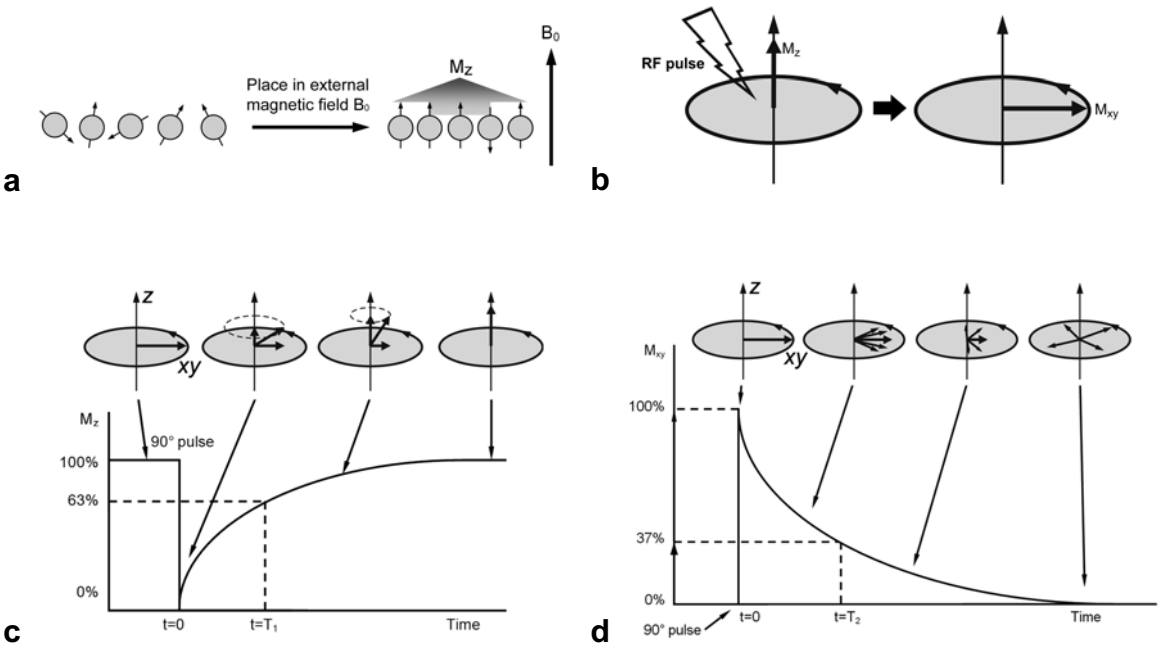

Figure 2.1: MR basics. (a) Protons (^1H) possess a magnetic moment, or "spin". When placed in an external field B_0, the majority of these spins align parallel to B_0 (along the z-axis), resulting in a magnetization vector M_z. (b) Application of a 90° RF pulse flips M_z into the xy-plane (perpendicular to B_0), resulting in magnetization vector M_{xy} and phase coherence between spins. (c) M_z will return to its original distribution along the z-axis through T_1 relaxation (eq. 2.3). (d) Loss of phase coherence, and thereby loss of magnetization in the xy-plane, is determined by T_2 relaxation (eq. 2.4).

After application of a 90° pulse the magnetization vector will be in the *xy*-plane, and the spins will be in phase coherence; M_z will be zero and M_{xy} will be at a maximum (Fig. 2.1b). This process is commonly referred to as pulse excitation. After the RF pulse is switched off, the net magnetization vector will start reverting back to its equilibrium state as a result of a process which is called relaxation. The recovery process along the longitudinal axis is called T_1 relaxation, spin-lattice relaxation or longitudinal relaxation (Fig. 2.1c) and is described as:

$$M_z(t) = M_{z_{\max}} \left(1\text{-}e^{-\frac{t}{T_1}}\right) \tag{2.3}$$

During this process, the nuclei are giving up energy to their immediate surroundings. The dephasing process in the transverse plane (the plane orthogonal to B_0) is referred to as T_2 relaxation, or spin-spin relaxation.

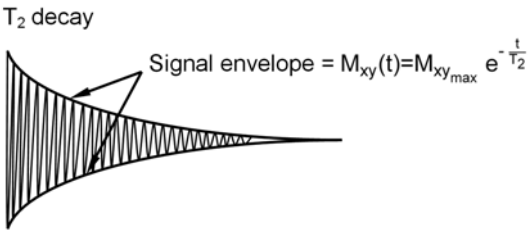

Figure 2.2: Free induction decay; after a single RF pulse the signal detected in the transverse plane is sinusoidal in shape and decays to zero over time under influence of the transverse relaxation.

In this process, nuclei exchange energy with each other and the spins lose phase coherence. To first order the net magnetization in the *xy*-plane decays exponentially to zero over time. The rate at which this occurs is dependent on T_2 (Fig. 2.1d) and the T_2 process is described as:

$$M_{xy}(t)=M_{xy_{\max}}\, e^{-\frac{t}{T_2}}. \tag{2.4}$$

In reality the signal will decay at a faster rate than T_2 due to field inhomogeneities and magnetic susceptibility differences. This shorter relaxation rate is known as T_2^*, and can be determined according to

$$\frac{1}{T_2^*}=\frac{1}{T_2}+\frac{1}{T_{2\mathrm{M}}}+\frac{1}{T_{2\mathrm{MS}}}. \tag{2.5}$$

Here $T_{2\mathrm{M}}$ is the dephasing due to inhomogeneity of the applied field, and $T_{2\mathrm{MS}}$ is the dephasing due to magnetic susceptibility differences (4).

An RF coil placed in the transverse plane will detect the transverse component of the net magnetization vector as it precesses around B_0. The length of the magnetization vector is the magnitude of the signal, while the angle between the magnetization vector and the *y*-axis is referred to as the phase of the signal. The decaying sinusoidal signal detected in the transverse plane (Fig. 2.2) after a single RF pulse is known as the free induction decay. Depending on the sample the FID can contain multiple resonance frequencies. A simple spectrum can be obtained from the FID by converting it from the time domain to the frequency domain using the Fourier transform. The resulting spectrum contains peaks for the various different frequencies contained within the FID.

2.1 Magnetic Resonance Imaging

In the above model where nuclei are placed in a homogeneous magnetic field, and an RF excitation pulse is followed by relaxation of the nuclei, the entire sample would only give a single signal. In other words, in the above highly simplified system, the NMR signal

cannot be spatially resolved. In order to assign spatial information to smaller volume units, commonly denoted as voxels, an additional step is required. From the basic equation in the previous section, it is clear that the resonance frequencies of spins depend on the magnetic field strength in which they reside. Spatial variations in frequencies can be translated to spatial information and subsequently to an image. Assigning spatial information to the spins is achieved by adding a magnetic field gradient inside the MR scanner. The gradient field is parallel to B_0 and its strength varies with position relative to B_0. The gradient has three components, G_x, G_y, and G_z, associated with the x, y, or z spatial axis, respectively. The spins experience different field strengths depending on where they are within the gradient field. Positional dependence of the field strength and resonance frequencies can be calculated according to:

$$B(\boldsymbol{r})=B_0+\boldsymbol{rG} \tag{2.6}$$

$$\omega(\boldsymbol{r})=\gamma B(\boldsymbol{r})=\gamma B_0+\gamma\boldsymbol{rG} \tag{2.7}$$

Here $B(\boldsymbol{r})$ and $\omega(\boldsymbol{r})$ are the position dependent field strength and resonance frequency, respectively. The position in the magnetic field is denoted by the vector $\boldsymbol{r}$ and the magnitude and direction of the gradient as $\boldsymbol{G}$ (2,4). Spins in different volume units within the field gradient experience a different magnetic field. Each "sub-field" is associated with a different Larmor frequency. The initial localization step is most commonly in the selection of the desired cross-section or "slice". This is achieved by applying a gradient along the z-axis in combination with an excitation pulse. This RF pulse excites only the spins in the desired slice, while leaving adjacent spins unaffected, as they have a different resonance frequency due to the applied z-gradient. Within the acquired slice, the x- and y-gradients are applied to assign the spins at each position within the slice with a unique frequency and phase. The gradients in this example are often referred to as the ***slice selection-*** (G_z), the ***frequency encoding-*** (G_x) and the ***phase encoding gradients*** (G_y). G_x is usually kept constant over the course of an experiment, thus assigning a different frequency to each position along the x-axis. G_y is stepped a number of times each scan, depending on the desired resolution in the y-direction. G_y applies a specific phase angle to the transverse magnetization vector. While G_y is switched on, each transverse magnetization vector has its own unique Larmor frequency. When G_y is subsequently switched off, the spins return to the frequency they had prior to phase encoding, however, the phase angle of each transverse magnetization vector is different. A variety of imaging pulse sequences can be created by combining slice selection, phase encoding and frequency encoding. In two-dimensional experiments, all three of the above components

are used in an orthogonal manner. In true 3D imaging experiments, two phase encoding directions and one frequency encoding direction are used.

Among the most important and widely used pulse sequences for MRI are the spin echo sequence and the gradient echo sequence. GE sequences use a slice selective pulse of 90° or less, and subsequently employ the gradient coils for producing an echo. This is done by first applying a negative frequency-encoding gradient, which is subsequently reversed, causing the spins to rephase and form an echo. Following signal detection the phase coherence of the precessing spins in the transverse plane is dephased or "spoiled" using spoiler gradients, thus ensuring contribution of only the longitudinal magnetization to the net magnetization $\boldsymbol{M}$ at the time of the next excitation pulse (4). Conversely, SE sequences use a slice selective 90° pulse for excitation, followed by a 180° pulse at t = TE/2. The 180° pulse serves to reverse or refocus the spins. This produces an echo at t = TE. During SE acquisition, the phase encoding gradient is applied following the 90° pulse, and the frequency encoding, or read out-, gradient is applied centered around the echo at t = TE (4). The TE in these examples is the echo time, and is measured from the center of the excitation pulse to the center of the echo. As multiple excitation-refocus-echo steps are needed to build up an entire image, the sequence is looped several times, depending on the desired resolution. The repetition time is defined as the time from the start of one loop of the sequence to the next.

2.1.1 Rapid acquisition with relaxation-enhancement imaging

Rapid acquisition with relaxation-enhancement imaging (5) is a fast spin echo imaging sequence in which multiple spin echoes are generated by employing multiple 180° refocusing pulses (Fig. 2.3). Each refocused echo is acquired after having experienced a different phase-encoding value. Because refocusing of the transverse magnetization is inherent in the sequence, it is less vulnerable to susceptibility-induced dephasing than gradient echo sequences, but it is substantially faster to apply than a spin-echo sequence with a single-phase encoding step per repetition time.

The primary contrast is T_2-based, although this can be mixed with T_1 and perfusion effects by combining it with the inversion recovery sequence (IR-RARE). The contrast in the final image can be modified depending on the choice of TE and TR. Choosing a long TR, and a relatively long TE, for example, will yield a T_2-weighted image, where elements with long T_2 will appear bright, and elements with a short T_2 will appear dark. A practical implementation of RARE imaging in visualizing Alzheimer's Aβ plaques is demonstrated in chapter 3.

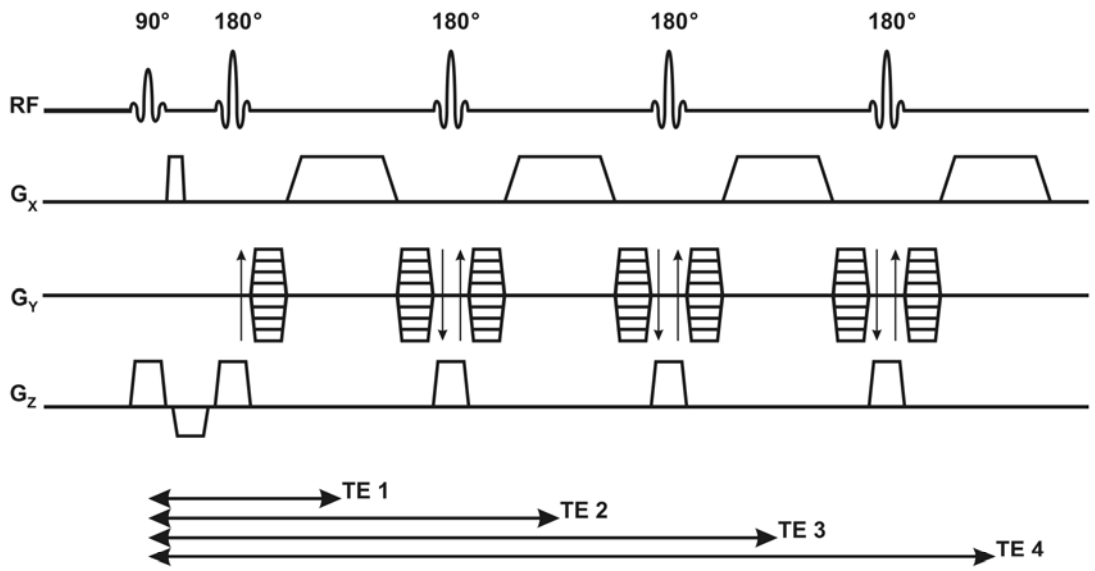

Figure 2.3: RARE pulse sequence: A four-segment (RARE factor of 4) version is shown. Each cycle has four phase encoding steps; the sequence will be looped until the desired number of phase encoding steps is reached. As this sequence acquires four times the data per loop as a standard SE sequence, the scan time is roughly 25% shorter than for an equivalent SE sequence. The effective TE is the TE time during which the G_y = 0 lines of data are acquired (4).

2.1.2 Transverse relaxation mapping

The relaxation times (T_2 and T_1) mentioned in the introductory section of this chapter may vary depending on tissue type, protein molecular structure, water content or presence of metal ions such as iron or manganese. As mentioned in chapter 1, disease mechanisms influence the composition of tissue, and can have an effect on the tissue specific relaxation rates. As AD pathology is predominantly visualized in MR research using T_2-weighted methods, T_2 mapping has been proposed as a tool to diagnose and/or predict AD (see chapter one).

Considering that the amount of magnetization present in the *xy*-plane depends on T_2, and that by modifying the TE value of a spin echo technique different T_2-weighting factors are obtained, it is possible to calculate the value of T_2 from a series of SE images with different echo times. As the signal intensity in these images is related to the magnetization in the *xy* plane, T_2 can be calculated by substituting the measured signal intensity for $M_{xy}(t)$, according to

$$M_{xy}(t)=M_{xy_{\max}}\, e^{-\frac{t}{T_2}}, \tag{2.8}$$

where t equals the experimental TE mentioned above.

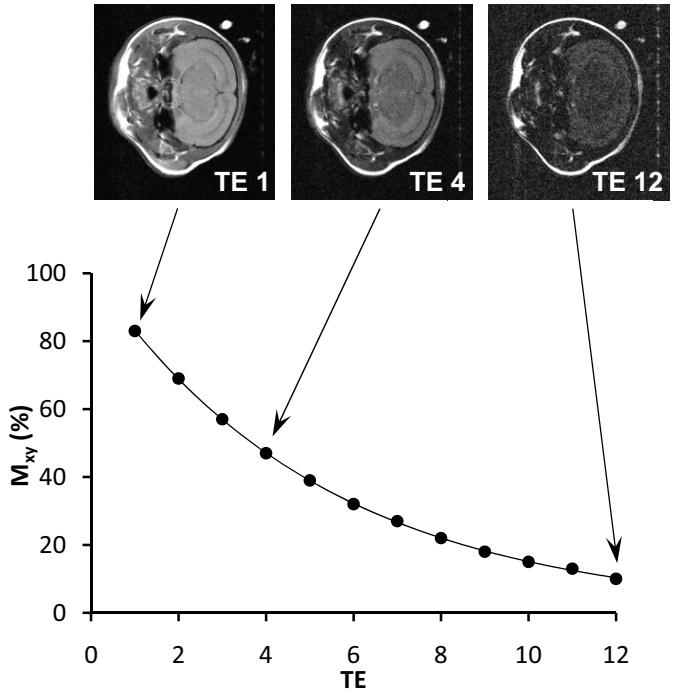

Figure 2.4: To calculate T_2 for specific regions of interest, a series of spin echo images is recorded, each with increasing TE. As TE increases, the signal intensity will decrease. This is plotted in the adjoining graph. An exponential decay function can be fit to this data, which allows calculation of the T_2 relaxation. As the transverse relaxation rate is calculated according to (eq 2.8), T_2 can be obtained in a relatively straightforward manner.

This can be calculated for the individual voxels of the sample, thus creating a T_2 map, or for specific regions of interest, by averaging the signal intensities for the pixels located within the ROI, and calculating the average T_2 for that region. Since an SE technique is used here, the signal is rephased before detection, which causes the effects of field inhomogeneities and susceptibilities to cancel. Hence, the calculated T_2 is the "true" T_2 and not T_2^*. Chapter 3 contains a practical implementation of this technique.

2.2 Magnetic Resonance Spectroscopy

The most basic method to obtain MR spectra is by placing a sample within the magnetic field of an MR scanner, exciting the spins in the sample by means of an RF pulse, and recording the FID as the spins relax back to their equilibrium state. Subsequent Fourier transformation of the recorded signal yields the magnetic resonance spectrum. Despite the numerous variations on this sequence that can be implemented, the obtained spectrum will always be of the entire sample within the scanner.

For *in vivo* applications it is desirable to localize the spectroscopic measurement in a specific volume of interest, or voxel. In the first *in vivo* experiments, the signal was approximately localized using a coil suitable for the observed organ, such as a surface coil to study the brain. However, a wide variety of more accurate spatial localization techniques using B_0 gradients have since been developed. These methods rely on the selection of spatially selective slices by the application of frequency-selective RF pulses

in the presence of a magnetic field gradient. Some of them require several acquisitions to achieve complete localization, whereas others can achieve localization in a single experiment (6), (Chap. 5). Among the most popular methods is point resolved spectroscopy (7,8). The PRESS sequence (Fig. 2.5a) is a double spin-echo sequence. Three slice-selective pulses (90°, 180°, 180°) along three orthogonal axes define three orthogonal slices, and make it possible to localize the signal in the voxel formed by the intersection of the three slices (Fig. 2.5b).

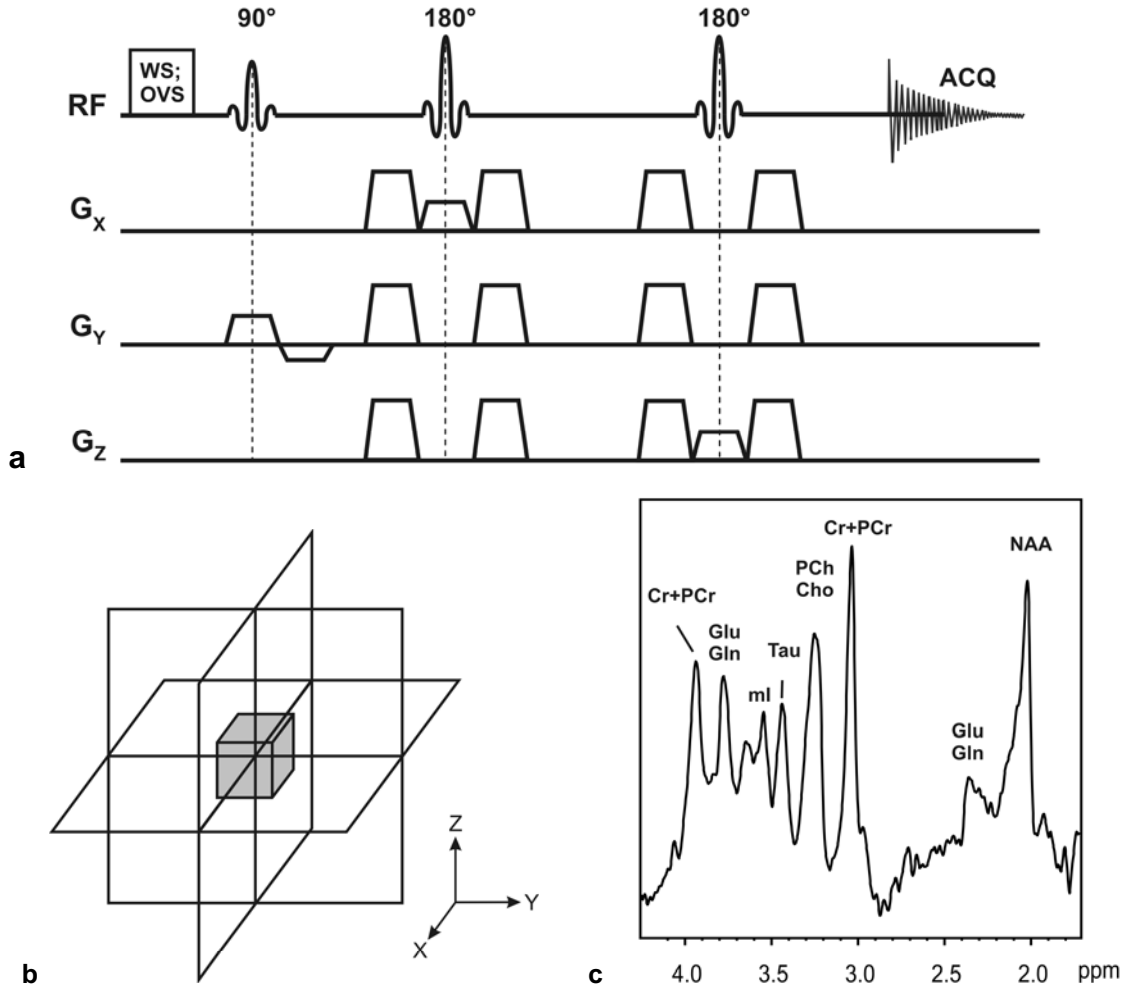

Figure 2.5: a) PRESS sequence: The slice selective pulses along orthogonal axes define three orthogonal slices, with the volume of interest (voxel) located at the intersection of the slices (b). The crusher gradients on either side of the 180° pulses dephase unwanted magnetization. The entire sequence is preceded by a water-suppression and outer volume suppression schemes. These remove the water signal and signals outside of the voxel from the final spectrum. c) An example of an MR spectrum obtained from a localized region in the brain of a mouse.

Outer volume suppression schemes excite narrow slices positioned around the volume of interest to selectively remove unwanted signals from outside the voxel. Following slice selective excitation, the transverse magnetization in these slices is dephased by a subsequent magnetic field crusher gradient. OVS is most commonly employed to remove lipid signals from the spectrum (3). As water is the most abundant compound in tissue, the NMR proton spectrum of almost all tissue is dominated by a resonance at ~4.7 ppm that originates from water protons. While metabolite detection is possible without water suppression, the water peak does lead to baseline distortions and spurious signals due to vibration-induced signal modulation, which make the detection of metabolites unreliable (3). Suppression of the water signal eliminates these problems, leading to a reliable and consistent detection of metabolite spectra. Water signals can be eliminated by utilizing differences in relaxation parameters. One such method, VAPOR, combines T_1-based water suppression and optimized frequency-selective perturbations to provide excellent water suppression with a large insensitivity towards T_1 and B_1 inhomogeneity (3,9). The combination of OVS and water suppression improves localization performance and reduces the demand for spoiler gradients (9).

When implementing MRS, in particular at ultra-high fields (≥ 7 Tesla), several important factors should be considered when preparing an experiment. The first is field inhomogeneity**.** A sample brought into the main magnetic field of the scanner distorts the magnetic field. Properly shimming the field prior to the experiment ensures that the magnetic field homogeneity is at its optimum. The need for a proper shim is that the resonance frequency of the sample depends on the magnetic field strength. Hence, spins "experiencing" the same field will resonate at the same frequency and thus produce a resonance with a narrow line, with a low FWHH. A poor shim will result in spins resonating at a range of frequencies rather than one single frequency, which in turn results in broad peaks and high FWHH. An additional benefit of narrow resonances is that the signal will be stronger, as the FWHH is inversely related to T_2 (10,11). The second important factor is short echo times**.** This criterion is closely related to the previous one, since T_2 relaxation rates increase with increasing field strength, yielding a shorter T_2. The choice of the shortest possible echo time ensures the least signal loss due to dephasing (10,11). Finally, the RF pulse bandwidth and gradient strength are important. Short, high bandwidth pulses, coupled with strong gradients are preferable, as these reduce the likelihood of chemical shift displacement artifacts (3,10,11).

2.3 Two-dimensional Magnetic Resonance Spectroscopy

The general idea of 2D experiments is to generate a second frequency axis by introducing an evolution delay into a pulse sequence, during which the transverse magnetization precesses at a different frequency than during signal acquisition (12,13). Generally, 2D MRS experiments consist of four stages: preparation, evolution, mixing and detection. Starting from a spin system in thermodynamic equilibrium, during the preparation period this spin system has to be prepared in a coherent non-equilibrium superposition of quantum states. One of the simplest 2D experiments is the correlation spectroscopy sequence (12,13). Here the preparation period consists of a single pulse. The spin system evolves during the evolution period t_1. To sample the changes during t_1, a series of experiments is carried out with a systematic increment of t_1. This provides the information in the frequency domain F_1 (13), (Chap. 6). During the mixing time a pulse is applied that transforms coherences into observable transverse magnetization. The observable magnetization is recorded during the detection time, commonly designated t_2, and corresponds to the other frequency domain in the 2D experiment. The experimental dataset collected therefore corresponds to a time domain matrix that comprises the time-dependent signals in the two time dimensions t_1 and t_2, and a double Fourier transform converts this into a matrix with two frequencies axes, F_1 and F_2. The result is a three-dimensional landscape representing the variation of the signal intensity over the plane spanned by the two frequency dimensions F_1 and F_2, and is commonly presented as a contour plot (14).

For the COSY experiment, incrementing the evolution period reveals the frequencies ω_1 during t_1 according to $\omega_1 = d\varphi/dt_1$, where φ is the phase of the coherences at $t_2 = 0$. For uncoupled spins the resonance frequency is identical during the evolution and detection period (i.e. $\omega_1 = \omega_2$), giving rise to diagonal peaks in the 2D MR spectrum. For *J*-coupled spin systems, additional off-diagonal or cross-peaks will arise at (ω_1, ω_2) and (ω_2, ω_1) where $\omega_1 \neq \omega_2$. This gives direct information on the connectivity pattern within a spin system via the *J*-couplings, and NMR signals can be assigned even when the spins are not resolved in the 1D spectrum (3), (Chap. 8).

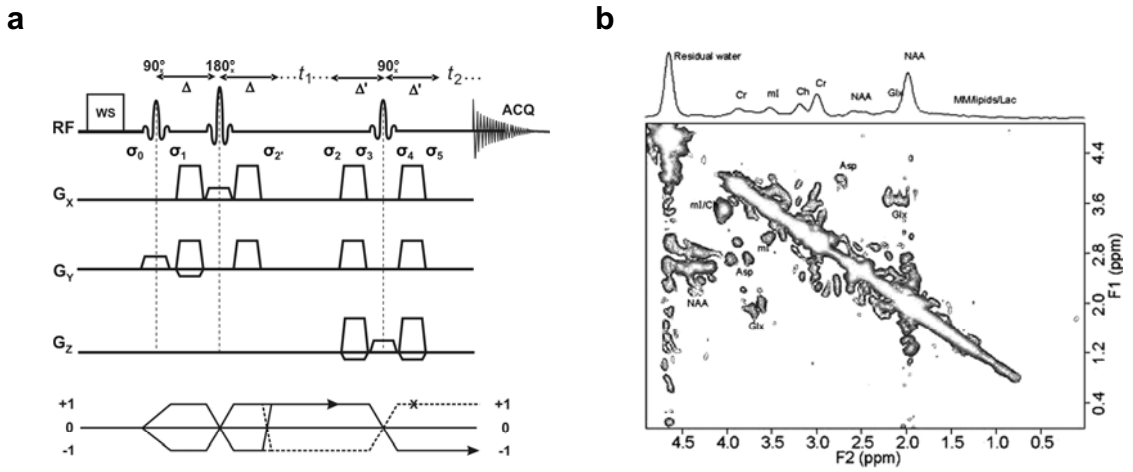

Figure 2.6: a) Localized two-dimensional shift correlated MR spectroscopic sequence. The RF pulse scheme consists of three RF pulses (90°, 180°, 90°), which are slice-selective along three orthogonal axes. A pair of B_0 gradient crusher pulses is symmetric with respect to the slice-refocusing 180° RF pulse. The last slice-selective 90° RF pulse with a pair of symmetric B_0 gradient crushers also serves as a coherence transfer pulse for the L-COSY spectrum. The sequence is preceded by a water suppression scheme. The coherence transfer pathway diagram depicts the different stages of conversion of magnetization/coherences (13). The t_1 evolution for the 2D spectroscopy, σ_2-σ_2, is integrated with volume localization and follows the evolution during the slice selection σ_1-$\sigma_{2'}$ that refocuses the chemical shift prior to the 2D evolution. b) Sample 2D L-COSY spectrum obtained from a 27 ml voxel localized in the occipito-parietal gray matter region of a healthy human volunteer. Reproduced, with permission, from Thomas et al. 2003 (15). © John Wiley & Sons, Inc.

Localized 2D shift-correlated MR spectroscopy (L-COSY)

In localized 2D MRS the preparation, evolution, mixing and detection are integrated with volume selection. The L-COSY sequence achieves this through the integration of an evolution period in a spatially selective PRESS sequence that comprises three slice selective RF pulses (90°, 180°, 90°) combined with three orthogonal B_0 gradients. The L-COSY sequence is derived from the COSY experiment and was first developed and published by Thomas and colleagues in 2001 (16). The pulse sequence with a representative 2D spectrum obtained from a localized region in the brain of a human subject is depicted in figure 2.6. The advantage of the L-COSY sequence is that the volume localization and the coherence transfer via the *J*-couplings are achieved simultaneously, without adding additional RF or gradient pulses. For high magnetic fields, the frequency differences between signals from different nuclear spins is often much larger than the scalar coupling constant *J*, and the spins are weakly coupled. In that case a straightforward description of the L-COSY experiment (Fig 2.6a) can be given using the product operator formalism instead of a full density matrix treatment. The calculation of the amplitudes and phases of L-COSY diagonal and cross peaks in a

weakly coupled two spin system, with *I* the spin under consideration and *S* its *J*-coupled partner (*I, S* = spin ½), is summarized below (3,13,16). The coherences σ_0-σ_5 describing the conversion of magnetization are depicted in Fig. 2.6a.

Prior to the first slice-selective 90° RF pulse, the preparation stage, the spin-state is represented by

$$\sigma_0 \propto I_z. \tag{2.11}$$

After the rotation by the first 90° RF pulse, the spin-state is represented by

$$\sigma_1 \propto I_y. \tag{2.12}$$

After the first evolution during the interval of 2Δ, the spins evolve under the influence of the gradients and *J*-coupling, but the chemical shift will be refocused by the slice selective 180° pulse resulting in an echo characterized by

$$\sigma_{2'} \propto I_y \cos(2\pi J_{IS}\Delta) - 2I_xS_z \sin(2\pi J_{IS}\Delta). \tag{2.13}$$

Starting from $\sigma_{2'}$, t_1 evolution allows for the encoding of chemical shift ($\omega_1^{(I)}$) for 2D spectroscopy, while in parallel the *J*-coupling sustains the development of the I_xS_z coherence for the detection of 2D correlations, yielding

$$\begin{aligned}\sigma_2 \propto & \left[I_y \cos\left(\omega_1^{(I)}t_1\right)\cos(\pi J_{IS}t_1) - 2I_xS_z \cos\left(\omega_1^{(I)}t_1\right)\sin(\pi J_{IS}t_1)\right.\\ & \left. - I_x \sin\left(\omega_1^{(I)}t_1\right)\cos(\pi J_{IS}t_1) - 2I_yS_z \sin\left(\omega_1^{(I)}t_1\right)\sin(\pi J_{IS}t_1)\right]\\ & \times \cos(2\pi J_{IS}\Delta) - \left[2I_xS_z \cos\left(\omega_1^{(I)}t_1\right)\cos(\pi J_{IS}t_1)\right.\\ & + I_y \cos\left(\omega_1^{(I)}t_1\right)\sin(\pi J_{IS}t_1) + 2I_yS_z \sin\left(\omega_1^{(I)}t_1\right)\cos(\pi J_{IS}t_1)\\ & \left. - I_x \sin\left(\omega_1^{(I)}t_1\right)\sin(\pi J_{IS}t_1)\right]\sin(2\pi J_{IS}\Delta).\end{aligned} \tag{2.14}$$

Using

$$A = \cos(\omega_1^{(I)}t_1)\cos(\pi J_{IS}t_1), \tag{2.14a}$$

$$B = \cos(\omega_1^{(I)}t_1)\sin(\pi J_{IS}t_1), \tag{2.14b}$$

$$C = \sin(\omega_1^{(I)}t_1)\cos(\pi J_{IS}t_1), \tag{2.14c}$$

$$D = \sin(\omega_1^{(I)}t_1)\sin(\pi J_{IS}t_1), \tag{2.14d}$$

eq. (2.4) simplifies to:

$$\sigma_2 \propto \left[AI_y\text{-}B2I_xS_z\text{-}CI_x\text{-}D2I_y\right]\cos(2\pi J_{IS}\Delta)\text{-}\left[A2I_xS_z\text{+}BI_y\text{+}C2I_yS_z\text{-}DI_x\right]\sin(2\pi J_{IS}\Delta). \quad (2.15)$$

A second pair of B_0 gradient crusher pulses is transmitted around the last slice-selective 90° RF pulse. After an evolution during the first set of crusher gradient pulses (θ_1), the spin state is represented by

$$\begin{aligned}\sigma_3 \propto \{&AI_y\cos\theta_1\text{-}AI_x\sin\theta_1\text{-}CI_x\cos\theta_1\text{-}CI_y\sin\theta_1\\ &\text{-}B2I_xS_z\cos\theta_1\text{-}B2I_yS_z\sin\theta_1\text{-}D2I_yS_z\cos\theta_1\\ &\text{+}D2I_xS_z\sin\theta_1\}\cos(2\pi J_{IS}\Delta)\text{-}\{BI_y\cos\theta_1\text{-}BI_x\sin\theta_1\\ &\text{-}DI_x\cos\theta_1\text{-}DI_y\sin\theta_1\text{+}A2I_xS_z\cos\theta_1\text{+}A2I_yS_z\sin\theta_1\\ &\text{+}C2I_y\cos\theta_1\text{-}C2I_xS_z\sin\theta_1\}\sin(2\pi J_{IS}\Delta). \end{aligned} \quad (2.16)$$

The spin state after the last 90° RF pulse rotation, or mixing stage, is

$$\begin{aligned}\sigma_4 \propto \{&AI_z\cos\theta_1\text{-}AI_x\sin\theta_1\text{-}CI_x\cos\theta_1\text{-}CI_z\sin\theta_1\\ &\text{+}B2I_xS_y\cos\theta_1\text{+}B2I_zS_y\sin\theta_1\text{+}D2I_zS_y\cos\theta_1\\ &\text{-}D2I_xS_y\sin\theta_1\}\cos(2\pi J_{IS}\Delta)\text{-}\{BI_z\cos\theta_1\text{-}BI_x\sin\theta_1\\ &\text{-}DI_x\cos\theta_1\text{-}DI_z\sin\theta_1\text{-}A2I_xS_y\cos\theta_1\text{-}A2I_zS_y\sin\theta_1\\ &\text{-}C2I_z\cos\theta_1\text{+}C2I_xS_y\sin\theta_1\}\sin(2\pi J_{IS}\Delta). \end{aligned} \quad (2.17)$$

At this point, evolution of I_z and $2I_xS_y$ will be excluded since there will be no observable signal. The spin state after an evolution during the last set of B_0 gradient crushers (θ_2):

$$\begin{aligned}\sigma_5 \propto &\text{-}\frac{1}{2}\cos(2\pi J_{IS}\Delta)\left[I_y\cos\left(\omega_1^{(I)}t_1\right)\cos(\pi J_{IS}t_1)\right.\\ &\text{+}I_x\sin\left(\omega_1^{(I)}t_1\right)\cos(\pi J_{IS}t_1)\text{+}2I_zS_x\cos\left(\omega_1^{(I)}t_1\right)\sin(\pi J_{IS}t_1)\\ &\left.\text{-}2I_zS_y\sin\left(\omega_1^{(I)}t_1\right)\sin(\pi J_{IS}t_1)\right]\text{+}\frac{1}{2}\sin(2\pi J_{IS}\Delta)\left[I_y\cos\left(\omega_1^{(I)}t_1\right)\sin(\pi J_{IS}t_1)\right.\\ &\text{+}I_x\sin\left(\omega_1^{(I)}t_1\right)\sin(\pi J_{IS}t_1)\text{-}2I_zS_x\cos\left(\omega_1^{(I)}t_1\right)\cos(\pi J_{IS}t_1)\\ &\left.\text{+}2I_zS_y\sin\left(\omega_1^{(I)}t_1\right)\cos(\pi J_{IS}t_1)\right]. \end{aligned} \quad (2.18)$$

Equation (2.8) shows the 2D encoding for the I-spin that was achieved during the t_1 period. It was calculated under the assumption that the gradient crushers are balanced ($\theta_1 = \theta_2$) and also using

$$\frac{1}{2\pi}\int_0^{2\pi}\cos\theta\sin\theta\,d\theta = 0 \quad \text{and} \quad \frac{1}{2\pi}\int_0^{2\pi}\sin^2\theta\,d\theta = \frac{1}{2}. \quad (2.19)$$

The phase factors, θ_1 and θ_2, are defined as:

$$\theta_1 = 2\pi\gamma \int \Delta B_0 d\tau_1 \text{ and } \theta_2 = 2\pi\gamma \int \Delta B_0 d\tau_2 \,. \quad (2.20)$$

Here τ_1 and τ_1 are the durations of the second pair of gradient crusher pulses. It is also evident from Equation (2.8) that the coherence transfer from spin *I* to spin *S* is characterized by $2I_zS_x$ and $2I_zS_y$. A similar equation can also be calculated for spin *S* resulting in a coherence transfer to spin *I*. Finally, the 2D signal acquired after the last crusher gradients, during the detection time t_2, is given by

$$s(t_1,t_2) = \mathrm{Tr}\ \{(I_x)\sigma_5\} e^{-i\omega_2^{(I)} t_2} e^{-t_1/T_2} \times e^{-t_2/T_2}\ [1-e^{-\mathrm{TR}/T_1}]. \quad (2.21)$$

A double Fourier transformation along both t_1 and t_2 axes will result in a 2D MR spectrum as a function of two frequency variables (F_1, F_2) described by:

$$S(F_1,F_2) = \iint s(t_1,t_2) dt_1 dt_2. \quad (2.22)$$

Aue *et al.* (17) reported that the diagonal peaks were dispersive, whereas the cross-peaks were absorptive when two hard 90° RF pulses were used to acquire the COSY spectrum. In contrast to the amplitude modulation in conventional COSY, phase modulation is present in the L-COSY, which is caused by the evolution during the B_0 gradient pulse before the last 90° RF pulse (18). Equation (2.8) clearly indicates that both the diagonal and cross-peaks of an L-COSY spectrum have mixed phases along the F_1 axis. Hence a drawback of including the gradient pulses is mixed line shapes in the 2D NMR spectra (18).

In this thesis the 2D L-COSY sequence has been applied for the first time in mouse brain, demonstrating its potential for simultaneously resolving and assigning several metabolite resonances *in vivo* (chapter 4) and examining the age-dependent neurochemical changes occurring in AD transgenic mice (Tg2576) as a result of disease progression (chapter 5).

References

1. Levitt MH. Spin Dynamics: Basics of Nuclear Magnetic Resonance, 1st ed. Wiley 2001, Chichester, UK.
2. Haacke EM, Brown RW, Thompson MR, Venkatesan R. Magnetic Resonance Imaging: Physical Principles and Sequence Design, 1st ed. Wiley-Liss 1999, Hoboken, USA.
3. De Graaf RA. In vivo NMR spectroscopy: Principles and techniques, 2nd ed. Wiley 2008, Chichester, UK.

4. Brown MA, Semelka RC. MRI: Basic Principles and Applications, 3rd ed. Wiley-Liss 2003, Hoboken, USA.
5. Hennig J, Nauerth A, Friedburg H. Rare Imaging - A Fast Imaging Method For Clinical Mr. Magn Reson Med 1986;3:823-833.
6. De Graaf RA. In vivo NMR spectroscopy: Principles and techniques, 1st ed. Wiley 1998, Chichester, UK.
7. Bottomley PA; Selective volume method for performing localized NMR spectroscopy, 1984; US patent 4,480,228
8. Bottomley PA. Spatial Localization In NMR Spectroscopy In vivo. Ann N Y Acad Sci 1987;508:333-348.
9. Tkac I, Starcuk Z, Choi IY, Gruetter R. In vivo H-1 NMR spectroscopy of rat brain at 1 ms echo time. Magn Reson Med 1999;41:649-656.
10. Tkac I. Lecture notes: The Ingredients of a Successful MRS Study at Ultra-High-Field. ISMRM 16th annual meeting 2008. Toronto, Canada.
11. Tkac I, Gruetter R. Methodology of H-1 NMR spectroscopy of the human brain at very high magnetic fields. Applied Magnetic Resonance 2005;29:139-157.
12. Jeener J. unpublished lecture notes. Ampere Summer School 1971. Basko Polje, Yugoslavia.
13. Ernst RR, Bodenhausen G, Wokaun A. Principles of nuclear magnetic resonance in one and two dimensions. Oxford Publications 1987, Oxford, UK.
14. Martin GE, Zektzer AS. Two-dimensional NMR methods for establishing molecular connectivity. VCH Verlagsgesellschaft 1988, WeinHeim, Germany.
15. Thomas MA, Hattori N, Umeda M, Sawada T, Naruse S. Evaluation of two-dimensional L-COSY and PRESS using a 3 T MRI scanner: from phantoms to human brain in vivo. NMR Biomed 2003;16:245-251.
16. Thomas MA, Yue K, Binesh N, Davanzo P, Kumar A, Siegel B, Frye M, Curran J, Lufkin R, Martin P, Guze B. Localized two-dimensional shift correlated MR spectroscopy of human brain. Magn Reson Med 2001;46:58-67.
17. Aue WP, Bartholdi E, Ernst RR. 2-Dimensional Spectroscopy - Application To Nuclear Magnetic-Resonance. J Chem Phys 1976;64:2229-2246.
18. Brereton IM, Galloway GJ, Rose SE, Doddrell DM. Localized 2-Dimensional Shift Correlated Spectroscopy In Humans At 2-Tesla. Magn Reson Med 1994;32:251-257.